Uluslararası Mühendislik Araştırma ve Geliştirme Dergisi
International Journal of Engineering Research and Development

UMAGD, (2021) 13(2), 635-644.

10.29137/umagd.896904

Cilt/Volume:13 Sayı/Issue:2 Haziran/June 2021

Araştırma Makalesi / Research Article

Dielectric Properties of BN-ZnO-GNP Doped PU-EG Composites

Safa Polat

Karabuk University, Material Research and Development Centre, 78050, Karabük, TURKEY

***Başvuru/Received**: 15/03/2021* ***Kabul / Accepted**: 19/05/2021* ***Çevrimiçi Basım / Published Online:** 02/06/2021*

***Son Versiyon/Final Version**: 18/06/2021*

Abstract

In this study, ZnO and GNP were added separately and together to improve the dielectric constant values of hexagonal boron nitride. Polyurethane (PU) and ethylene glycol (EG) were used as binders. The productions were carried out by dispersing each additive separately in acetone and then coating it with the doctor blade method on aluminium foil. The characterizations were carried out with FTIR, XRD and SEM. Then, the capacitance values of each composite were first measured with the LCR meter and then the dielectric constant were calculated. According to the results, the highest dielectric constant values were obtained at the 100 and 120 Hz frequencies. At the frequency value of 100 kHz, the lowest dielectric constant was obtained in all composites. Compared to pure BN, an increase of 115% was achieved with ZnO doping, while an increase of up to 145% was achieved with GNP doping. The highest increase was achieved up to 160% with ZnO + GNP doping. In addition, with the doping of ZnO + GNP, the amount of decrease at high frequencies was less than the others. This is thought to be due to the combined effect of both ZnO and GNP, which has a large surface area.

Key Words

"Graphene nanoplate, Zinc oxide, Boron nitride, Dielectric constant, Composite materials"

***Sorumlu Yazar:** safapolat@karabuk.edu.tr*

1. Introduction

With the increase of the human population and the depletion of natural resources, the demand for the clean energy sector has increased. Especially with the decrease in fossil and solid fuels, the use of electrical energy has gained importance in many areas (Strengers, 2013). One of these areas is the automotive sector (Bayod-Rújula et al., 2011). In recent years, it is aimed to significantly reduce the use of fossil fuels and environmental pollution in the world with the development of electric cars in this sector (Cusenza et al., 2019). For this purpose, many studies have been conducted in the scientific world on the storage of electrical energy to be used in such applications (Muratori, 2018). One of these studies is capacitors. Capacitors are systems where electricity is stored by accumulating charge on a dielectric material placed between two metal plates. In this system, polarization is created by applying an electric field to the dielectric material during charging. These polarizations create an electric current while returning to its former state (discharge) (Sun et al., 2014; Zhang, 2020). The materials developed based on this working principle have been put into use for the purpose of electrical energy storage especially for portable vehicles in recent years. One of the most important parameters affecting the storage capacity in such systems is known as the thickness of the dielectric material placed between two plates (Black and Welser, 1999). In order to reduce this thickness, various coatings consisting of different components have been applied to metal plate surfaces by using methods such as spin coating and deep coating (Dyer et al., 2010; Shin et al., 2007). However, such capacitors are known to be both low capacity and costly in the manufacturing process. In this context, the use of nanoparticle reinforced composites produced by simpler methods as dielectric material in capacitors has become widespread in recent years (Chan et al., 2019; Deshmukh et al., 2016; Wang et al., 2018). Especially, the thickness of the dielectric material and the surface area of the collectors are very important. In this context, the use of plate-shaped microparticles such as hexagonal boron nitride in capacitors enables the formation of micro-sized cells and thus higher capacitance values. However, although boron nitride has a geometric advantage, its dielectric coefficient is quite low. In this context, higher energy storage can be achieved by increasing the dielectric and capacitance values. In addition, thanks to semiconductors such as SiO_2 CuO, $BaTiO_3$ and $SrTiO_3$ the load storage capacity can be improved by increasing the dielectric coefficient of such materials (Akinay and Akkuş, 2020, 2019; Wang et al., 2020). However, since there is a need for more energy storage in recent years, it is desired that such ceramics have higher electrical storage capacities. It is known that products developed with nano technology, which are innovative and provide more efficiency compared to products developed with traditional productions, provide very beneficial results in this field. It is observed that the development of large surface area nanoparticles such as carbon nanotube and graphene and their use together with dielectric materials significantly increase the capacitance values of ceramics (Deng et al., 2013). In addition, it is known that metal-based nanoparticles are also used in capacitors by adding dielectric material to increase capacitance (Lu et al., 2006).

Considering these results, it was aimed to add graphene and zinc oxide particles on hexagonal boron nitride particles, which have a plate-like microstructure. For this purpose, the effect of graphene in the form of a plate and ZnO, a semiconductor metal oxide, on capacitance and dielectric coefficient were examined separately and together. Ethylene glycol (EG) and polyurethane (PU) are used as binders in production. The characterizations of the products obtained were made with FTIR and SEM. After these processes, the capacitance values of each product were measured at five different frequencies using the LCR meter. Then, the dielectric coefficients of each are calculated and the results are discussed.

2. Materials and Method

Hexagonal boron nitride (hBN, 10 µm), graphene nano plates (GNPs, 5 µm, thickness of 5-8 nm and a surface area of 750 m^2/g), ZnO, acetone, polyurethane and ethylene glycol were utilized as raw materials without further purification. Boron nitride was purchased from HENZE BNP. Other materials, especially graphene, were purchased from Nanografi Nano Technology Inc.

In this study, firstly, four different containers were taken and numbered from 1 to 4. Then 0.35 g of h-BN was added to the first container. 0.315 g h-BN and 0.035 g ZnO were added to the second container. 0.315 g h-BN and 0.035 g GNP were added to the third container. 0.315 g h-BN, 0.0175 g ZnO and 0.0175 g GNP were added to the fourth container. Each of these containers was added 10 ml of acetone, covered with parafilm, and mixed in an ultrasonic bath for one hour (Fig. 1a). After this process, each was taken on a magnetic stirrer and 3 ml of polyurethane and 3 ml of ethylene glycol were added as binders and the acetone was removed by stirring at approximately 80-120 °C for a further period (Fig. 1b). The pasty mixtures obtained were placed on aluminum foil with the help of a spatula. Then, the mixture dough was covered with the doctor blade method on the foils [1]. In this method, briefly, firstly, binder polymers, solvent and powder mixtures are combined in a container in determined proportions and mixed until a homogeneous slurry is obtained. Then, the aluminum foil is cut in the specified size and adhered to a hard and smooth surface and the surface is cleaned with alcohol and acetone. Then, one end of the area to be covered is adhered with tape so that it remains open. After this process, the prepared mud is put on the foil and a knife or stick is pressed on it and moved towards the open end. Thus, coating is performed on the foil surface. After applying the same method for each, the foils were dried in a 70 °C oven for one day. After this process, each was cut separately in suitable dimensions. The foils on the underside of the cut plates serve as conductor collectors. Conductivity was ensured by sticking a conductive carbon tape on the upper sides as shown in Fig. 1c. Capacitance measurements were made by attaching one of the alligator copper cables coming from the LCR meter to foil and the other to the carbon tape. Measurements were carried out at frequencies of 100 Hz, 120 Hz, 1 kHz, 10 kHz, and 100 kHz. After this process, the dielectric coefficient of each composite was calculated according to the formula given in equation 1 (Rao et al., 2002).

$$C = (\varepsilon_0 \varepsilon_r)\mathrm{A/t} \quad (1)$$

Where ε_0 is the dielectric constant of the free space (8.854×10^{-12} F/m), ε_r, A and t are the dielectric constant, area and thickness of the composite materials, respectively.

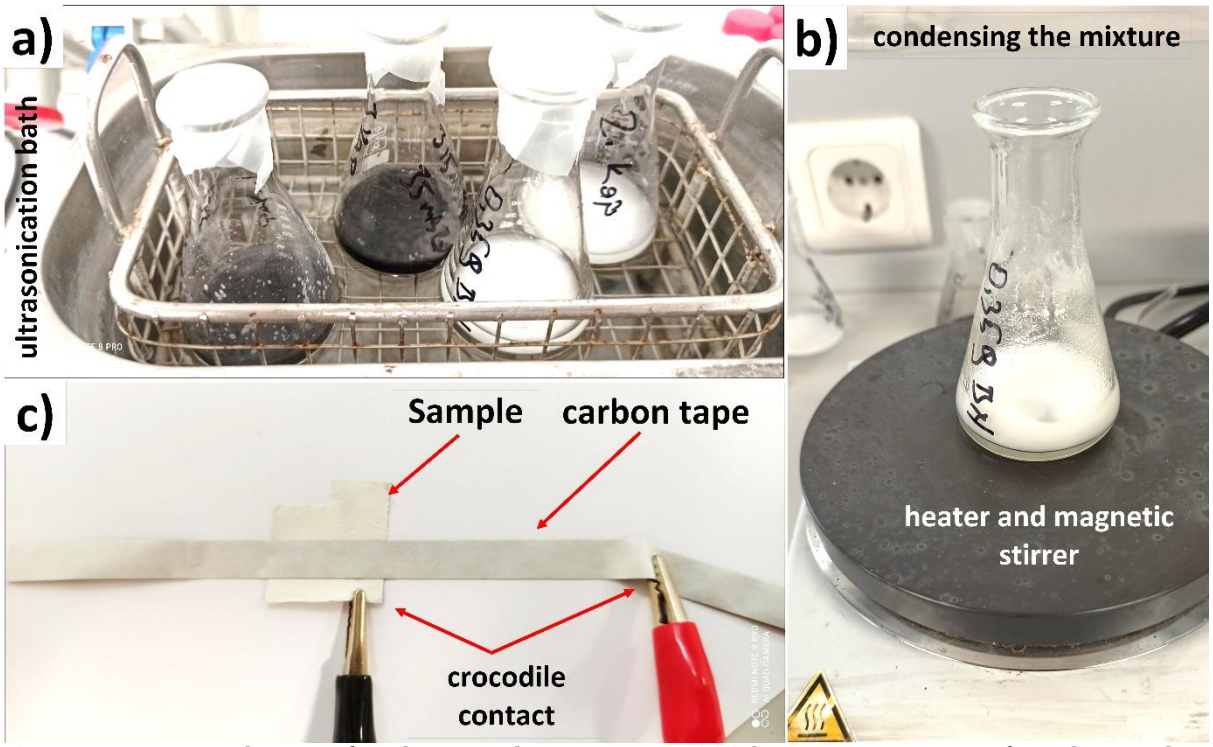

Figure 1. Experimental setups of production and measurements. **(a)** Ultrasonication process of powder particles. **(b)** Concentration of the mixtures by heating in a magnetic stirrer. **(c)** Measurement with LCR meter.

3. Results and Discussion

FTIR analysis was first performed for the characterization of composites. The obtained results are given in Fig. 2 and 3. Fig. 2 shows the spectra of the raw materials used for composites. When the spectrum of the powder particles is evaluated, it is understood that the sharp and flat peaks at 768 cm^{-1} and 1363 cm^{-1} belong to the boron and nitrogen bond (Kong et al., 2019). The peaks observed at 492 cm^{-1} and 560 cm^{-1} correspond to the bond between zinc and oxygen (Handore et al., 2014). The unclear peak observed around 1530 cm^{-1} belongs to the carbon-carbon bond from graphene (Peng et al., 2013). The other two spectrums are the characteristic peaks of ethylene glycol (Nohra et al., 2016) and polyurethane (Caddeo et al., 2015) raw materials. These include the OH bond at approximately 3300 cm^{-1} and the CH bonds at 2870 and 2942 cm^{-1}. Other characteristic peaks belong to the C = O bond in 1730, 1016 and 1088 cm^{-1}. Apart from these, it belongs to the C-O-C, N-H and C-N bonds observed in 1066, 1228, 1458 and 1530 cm^{-1}, respectively. When looking at the peaks obtained from composites in the light of these data, the sharp peak at 768 cm^{-1} and the broad peaks observed in 1363 cm^{-1} belong to the B-N bond. This situation confirms that boron nitride is used in composites. On the other hand, the peaks of ZnO observed at 492 and 560 cm^{-1} of BN + ZnO composites confirm the use of zinc oxide in this composite. However, the ZnO peak in the BN + ZnO + GNP composite is observed at a very low intensity, which is due to the lower amount of ZnO in it. Carbon bonds for graphene-containing composites could not be distinguished due to the carbon bond in ethylene glycol and polyurethane. Verification of this is discussed in the microstructure images.

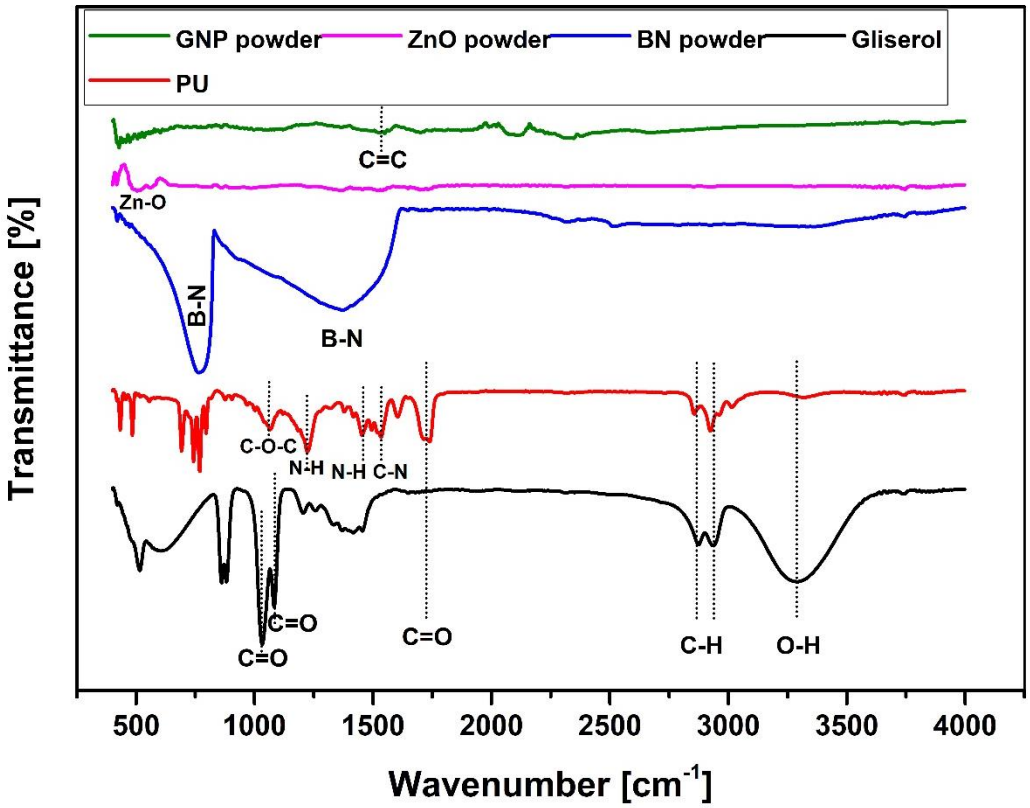

Figure 2. FTIR spectra of raw materials

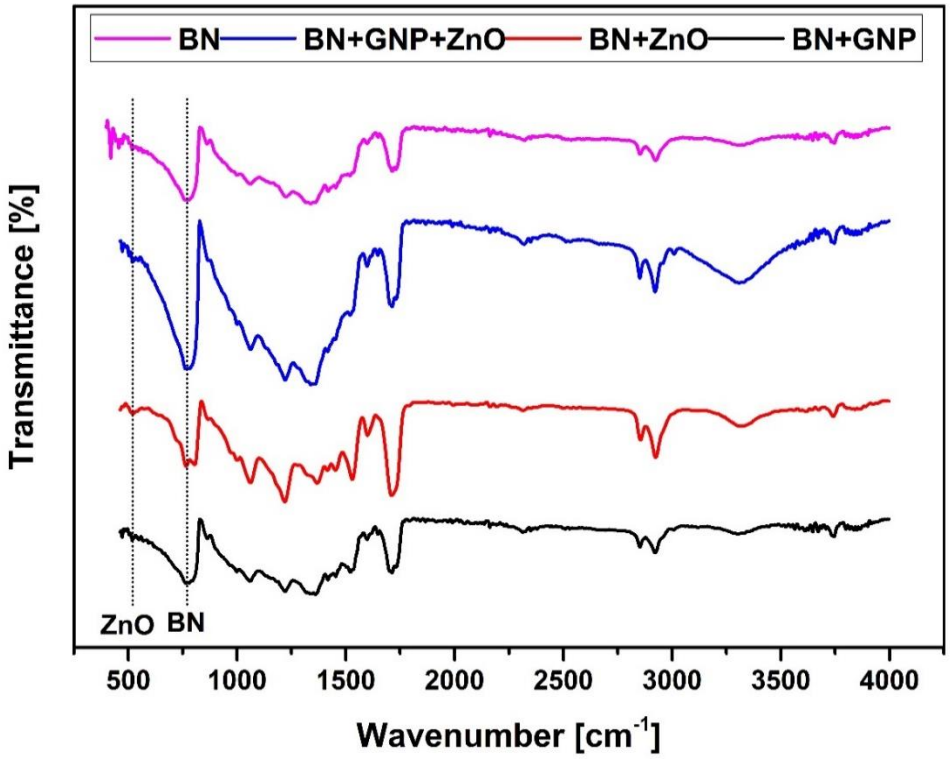

Figure 3. FTIR spectra of composite materials

XRD analysis results of powder mixtures are given in figure 4. According to the results of this analysis, it is understood that the sharp peaks observed at 2θ value approximately 31 °, 34 ° and 36 ° belong to the planes (100), (002) and (101) of ZnO, respectively. Also, low intensity peaks observed at approximately 47 °, 56 °, 62 °, 66 °, 67 ° and 68 ° belong to the (102), (110), (103), (200), (112) and (201) planes of ZnO, respectively (Zak et al., 2011). Apart from these, the severe peak observed at about 26 ° belongs to the hexagonal structure BN and GNP (Niftaliyeva et al., 2018; Zak et al., 2011). These two peaks coincide because the structures and planes of both are the same. However, the peaks of ZnO are quite distinct. Therefore, unlike the others, peaks of ZnO were observed in powder mixtures with ZnO additive. As a result, the observation of the characteristic peaks of the powder mixtures shows the accuracy of the components used. Since no extra new peak formation was observed, it can be said that no reaction took place during the mixing process.

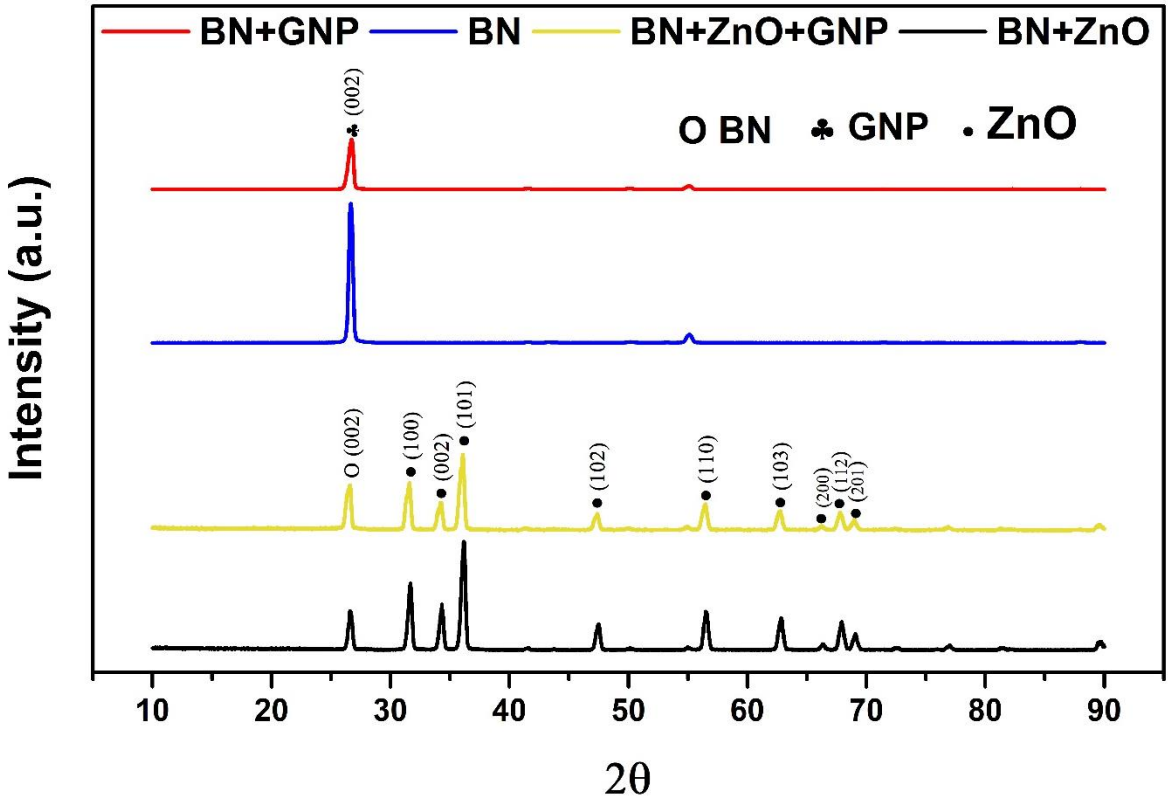

Figure 4. XRD pattern of powder mixtures

SEM images of powder particle mixtures are given in Figure 5. The surface images of boron nitride particles without any doping are given in Figure 5a. It is clear from this image that the BN surface is quite smooth and in the form of a plate. In Figure 5b, images of the ZnO-doped BN samples are given. From these images, it is understood that the ZnO particles are almost nano-sized rod-shaped, but they cluster due to electrostatic interaction and precipitate on the BN surfaces. In Figure 5c, BNs doped with nano-sized graphene plates are observed. Since GNP and BNs have the same microstructure image, it is very difficult to distinguish both structures from each other. However, here an image of nano-thick graphene plates intertwined with BN particles was obtained. Based on these images, it can be said that the interaction of GNP and BN has occurred quite well. On the other hand, in figure 5d, the picture of the mixture of BN + ZnO + GNP is given. In this image, it is observed that almost nano-sized rod-shaped ZnO are scattered between BN plates together with GNP. It is understood that these ZnO rods are formed by adding a nano-sized component to the mixture. The reason for this is thought to be that the nano-sized graphene plates were separated by penetrating between the clumped ZnO rods (Bayod-Rújula et al., 2011). In this way, it is observed that all three structures interact more with each other. On the other hand, the microstructure image of the composites obtained by mixing these micro and nanoparticles with polyurethane and ethylene glycol and spreading on aluminum foil is given in figures 6a and b. The image here shows that the particles are homogeneously distributed in the polymer, but porosity is also included. Two of the most important reasons for the occurrence of such porosities are viscosity and the other is shrinkage in the polymer during drying (Krokida et al., 1998; Schulze et al., 2003). As the amount of particles reinforced into the polymer increases, the viscosity also increases and therefore it solidifies rapidly without filling all the spaces during shaping. In addition, during the solidification by drying, some volumetric shrinkage occurs in the polymer and this causes the formation of voids in the structure. On the other hand, the low amount of binder compared to supplements is thought to have caused such porosities. However, it is found successful because it enables the particles to be found in bulk.

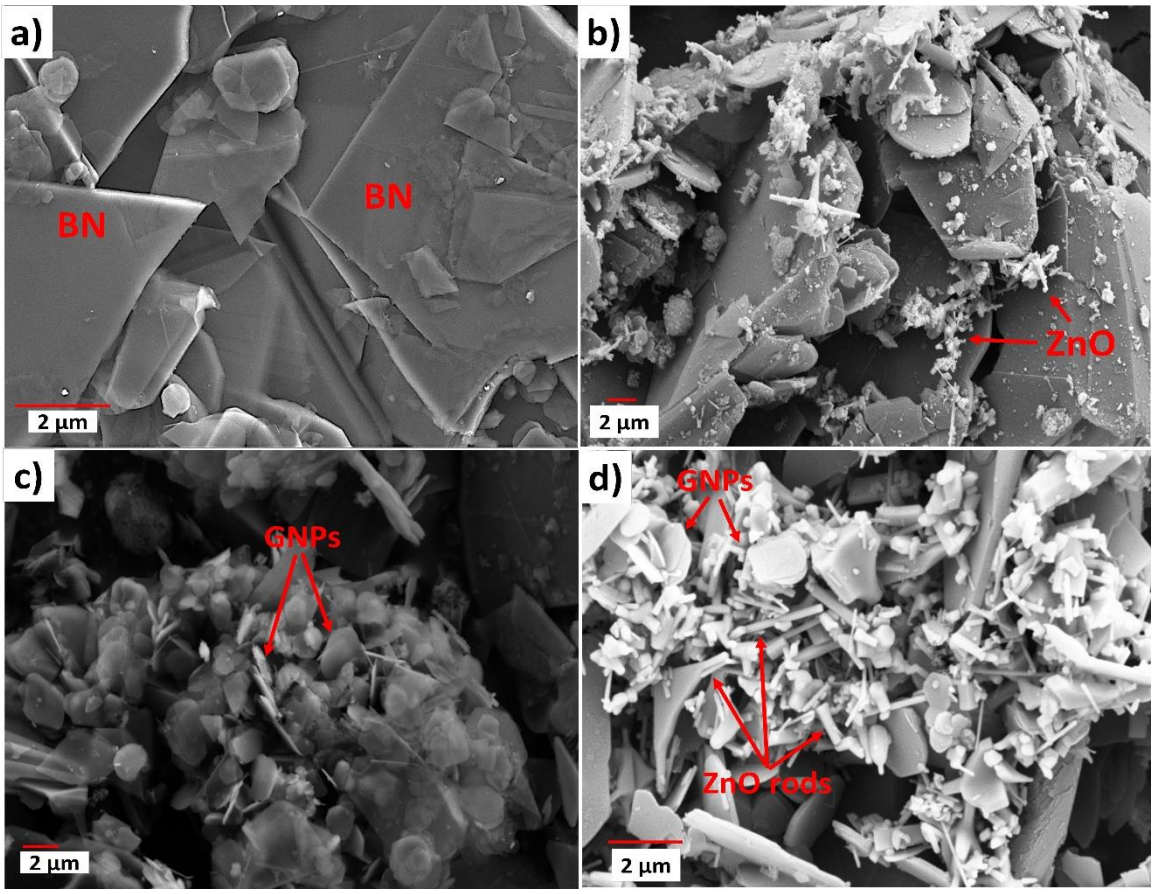

Figure 5. SEM images of powders. **(a)** BN. **(b)** BN + ZnO. **(c)** BN + GNP. **(d)** BN + ZnO + GNP. **(k and l)** Composite of BN + ZnO + GNP

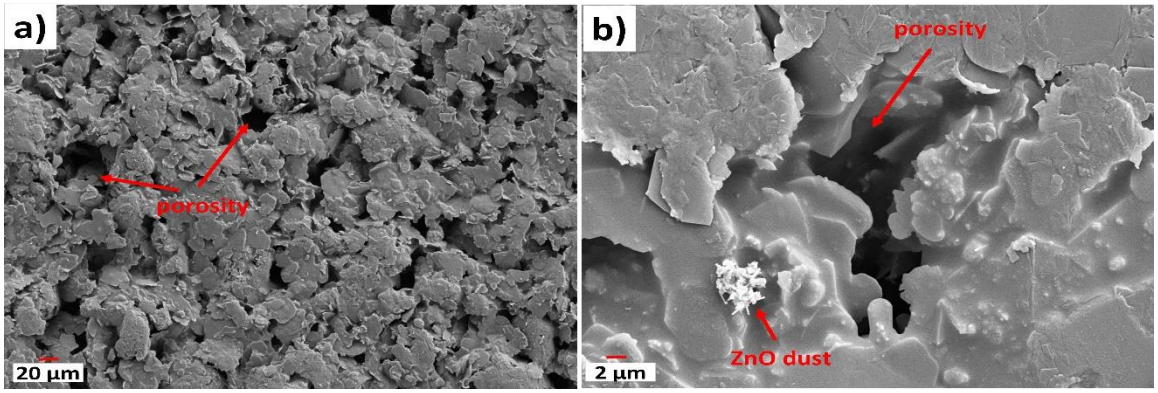

Figure 6. (a and b) Images of polyurethane + BN + ZnO + GNP composites at different magnifications

As for the dielectric and capacitance values of composites, each is given in table 1 in detail. According to these results, the graph created with the dielectric coefficient values against the frequency change of each composite is given in Fig. 7. According to these results, the highest dielectric coefficient for all composites is at 100 Hz, which is the lowest frequency. Among them, pure BN-doped composites are approximately 2.2, BN + ZnO-doped has 4.75, BN + GNP-doped has 5.4, and BN + ZnO + GNP-doped is 5.65. When compared with pure BN, it is calculated that there is 115% increase with ZnO doping, 145% increase with GNP doping and 156% increase with ZnO + GNP doping. When the frequency was increased to 120 Hz, the increase in percentage was calculated to be almost the same. However, when the frequency was increased to 1 kHz, there was an increase of 64% with ZnO doping, 120% with GNP doping and 160% with ZnO + GNP doping compared to pure BN. When the frequency was at 10 kHz, the doping of ZnO reached 4%, GNP doping reached 40% and ZnO + GNP doping reached 193%. Similarly, at 100 kHz, it increased 3% with ZnO, 9% with GNP and 147% with ZnO + GNP compared to BN. According to these results, as the frequency value increased, the dielectric coefficient values

of all composites decreased significantly, especially after 1 kHz. Although the dielectric coefficient is increased at low frequencies compared to BN with ZnO doping, it is in very low amounts at high frequencies. The GNP doping increased the dielectric coefficient significantly more than ZnO, especially up to 10 kHz. Apart from these, there is an exception that the percentage increase does not decrease as the frequency increases, which is the combined doping of ZnO + GNP. Although the doping of these components together decreases due to the frequency increase, it is quite high compared to pure BN. In this context, it can be said that the most successful results are with doping of ZnO + GNP. It can be said that the second most successful was the GNP doping and the last was ZnO. ZnO is thought to increase the values of BNs due to the height in its dielectric coefficient. GNP, on the other hand, is thought to contribute by creating nano-cells in series and parallel between BN plates, as it is conductive plates and spread over a large surface area. When ZnO particles with higher dielectric coefficient compared to BN were added between these plates, a synergistic effect was created, and higher dielectric coefficient results were obtained than all combinations.

When it comes to the comparison of the results with the literature, in this context, Çıracı et al. carried out a similar study and their results are quite consistent with our findings (Cusenza et al., 2019). In another study, the change in capacitance depending on the frequency was examined and according to the results it was found that the capacitance value at low frequencies was higher. It has been said that the reason for this is that at low frequency, the net polarization of the material increases because the electrons jump more easily, and this causes an increase in capacitance. However, at higher frequencies, it has been stated that the relaxation time of the charge carrier is not as fast as the change of the electric field with time, which has been reported to cause a decrease in capacitance (Muratori, 2018; Zhang, 2020). In this study, it is thought that a similar situation exists because the highest capacitance values are obtained at low frequencies.

Table 1 Sample parameters, measurement, and calculation results (C, ε_0, ε_r A, t = the capacitance, dielectric constant of free space, dielectric constant, area and thickness of the composite materials, respectively).

BN					
	100Hz	**120Hz**	**1kHz**	**10kHz**	**100kHz**
C	7.30E-11	7.20E-11	6.50E-11	3.00E-11	2.30E-11
ε_0	8.85E-12	8.85E-12	8.85E-12	8.85E-12	8.85E-12
ε_r	2.21E+00	2.18E+00	1.96E+00	9.06E-01	6.95E-01
A	0.000486	0.000486	0.000486	0.000486	0.000486
t	0.00013	0.00013	0.00013	0.00013	0.00013
BN + ZnO					
	100Hz	**120Hz**	**1kHz**	**10kHz**	**100kHz**
C	1.46E-10	1.42E-10	9.90E-11	2.90E-11	2.20E-11
ε_0	8.85E-12	8.85E-12	8.85E-12	8.85E-12	8.85E-12
ε_r	4.75E+00	4.62E+00	3.22E+00	9.44E-01	7.16E-01
A	0.000486	0.000486	0.000486	0.000486	0.000486
t	0.00014	0.00014	0.00014	0.00014	0.00014
BN + GNP					
	100Hz	**120Hz**	**1kHz**	**10kHz**	**100kHz**
C	5.20E-11	5.20E-11	5.00E-11	4.74E-11	4.35E-11
ε_0	8.85E-12	8.85E-12	8.85E-12	8.85E-12	8.85E-12
ε_r	6.23E+00	6.23E+00	5.99E+00	5.67E+00	5.21E+00
A	0.000066	0.000066	0.000066	0.000066	0.000066
t	0.00007	0.00007	0.00007	0.00007	0.00007
BN + GNP + ZnO					
	100Hz	**120Hz**	**1kHz**	**10kHz**	**100kHz**
C	7.90E-11	7.60E-11	7.20E-11	3.70E-11	2.40E-11
ε_0	8.85E-12	8.85E-12	8.85E-12	8.85E-12	8.85E-12
ε_r	5.65E+00	5.44E+00	5.15E+00	2.65E+00	1.72E+00
A	0.0003	0.0003	0.0003	0.0003	0.0003
t	0.00019	0.00019	0.00019	0.00019	0.00019

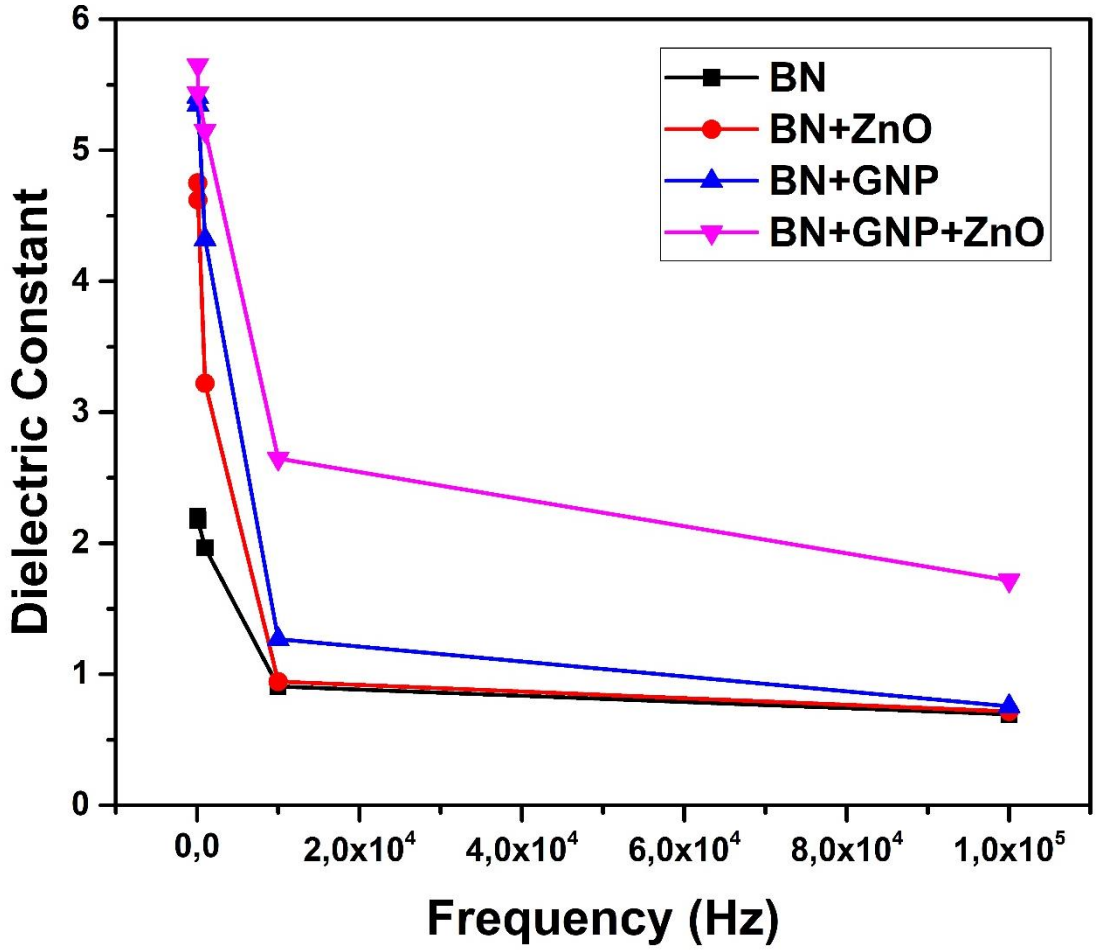

Figure 7. Plot of change in dielectric constant with frequency

4. Conclusion

According to the results obtained. the production of hexagonal boron nitride plates with ZnO and GNP additives with polyurethane and ethylene glycol binders has been successfully carried out. All of the materials used as raw materials and made into composite in characterizations with FTIR have been successfully verified. The combination states of these materials are shown in detail in the microstructure images. In the dielectric coefficient results. it was observed that all dopings increased around 115% to 160% at low frequencies. while this increase decreased in others except ZnO + GNP as the frequency increased. As a result. when ZnO and GNP are evaluated separately. it is understood that GNP is superior. but ZnO + GNP is the most successful composition. It is concluded that this is due to the synergistic effect of ZnO. which is located between GNP nanoplates and has a higher dielectric coefficient value than BN.

References

Akinay, Y., Akkuş, I.N., 2020. Synthesis and characterization of the pearlescent pigments based on mica deposited with SiO2, AlN and TiO2: First report of its dielectric properties. Ceramics International 46, 17735–17740.

Akinay, Y., Akkuş, I.N., 2019. The optic and dielectric properties of CuO deposited barite pigments. Academic Perspective Procedia 2, 1325–1330.

Bayod-Rújula, Á.A., Lorente-Lafuente, A.M., Cirez-Oto, F., 2011. Environmental assessment of grid connected photovoltaic plants with 2-axis tracking versus fixed modules systems. Energy 36, 3148–3158.

Black, C.T., Welser, J.J., 1999. Electric-field penetration into metals: consequences for high-dielectric-constant capacitors. IEEE Transactions on Electron Devices 46, 776–780.

Caddeo, S., Baino, F., Ferreira, A.M., Sartori, S., Novajra, G., Ciardelli, G., Vitale-Brovarone, C., 2015. Collagen/Polyurethane-Coated Bioactive Glass: Early Achievements towards the Modelling of Healthy and Osteoporotic Bone. Key Engineering Materials 631, 184–189. https://doi.org/10.4028/www.scientific.net/KEM.631.184

Chan, K.-Y., Yang, D., Demir, B., Mouritz, A.P., Lin, H., Jia, B., Lau, K.-T., 2019. Boosting the electrical and mechanical properties of structural dielectric capacitor composites via gold nanoparticle doping. Composites Part B: Engineering 178, 107480.

Cusenza, M.A., Guarino, F., Longo, S., Mistretta, M., Cellura, M., 2019. Reuse of electric vehicle batteries in buildings: An integrated load match analysis and life cycle assessment approach. Energy and Buildings 186, 339–354.

Deng, L., Hao, Z., Wang, J., Zhu, G., Kang, L., Liu, Z.-H., Yang, Z., Wang, Z., 2013. Preparation and capacitance of graphene/multiwall carbon nanotubes/MnO2 hybrid material for high-performance asymmetrical electrochemical capacitor. Electrochimica Acta 89, 191–198.

Deshmukh, K., Ahamed, M.B., Deshmukh, R.R., Pasha, S.K., Chidambaram, K., Sadasivuni, K.K., Ponnamma, D., AlMaadeed, M.A.-A., 2016. Eco-friendly synthesis of graphene oxide reinforced hydroxypropyl methylcellulose/polyvinyl alcohol blend nanocomposites filled with zinc oxide nanoparticles for high-k capacitor applications. Polymer-Plastics Technology and Engineering 55, 1240–1253.

Dyer, T.W., Cartier, E.A., Chudzik, M.P., Moumen, N., 2010. Deep trench (DT) metal-insulator-metal (MIM) capacitor.

Handore, K., Bhavsar, S., Horne, A., Chhattise, P., Mohite, K., Ambekar, J., Pande, N., Chabukswar, V., 2014. Novel Green Route of Synthesis of ZnO Nanoparticles by Using Natural Biodegradable Polymer and Its Application as a Catalyst for Oxidation of Aldehydes. Journal of Macromolecular Science, Part A 51, 941–947. https://doi.org/10.1080/10601325.2014.967078

Kong, D., Zhang, D., Guo, H., Zhao, J., Wang, Z., Hu, H., Xu, J., Fu, C., 2019. Functionalized Boron Nitride Nanosheets/Poly(l-lactide) Nanocomposites and Their Crystallization Behavior. Polymers 11, 440. https://doi.org/10.3390/polym11030440

Krokida, M.K., Karathanos, V.T., Maroulis, Z.B., 1998. Effect of freeze-drying conditions on shrinkage and porosity of dehydrated agricultural products. Journal of food engineering 35, 369–380.

Lu, J., Moon, K.-S., Xu, J., Wong, C.P., 2006. Synthesis and dielectric properties of novel high-K polymer composites containing in-situ formed silver nanoparticles for embedded capacitor applications. Journal of Materials Chemistry 16, 1543–1548.

Muratori, M., 2018. Impact of uncoordinated plug-in electric vehicle charging on residential power demand. Nature Energy 3, 193–201.

Niftaliyeva, A., Pehlivan, E., Polat, S., Avci, A., 2018. Chemical synthesis of single-layer graphene by using ball milling compared with NaBH4 and hydroquinone reductants. Micro & Nano Letters 13, 1412–1416.

Nohra, B., Candy, L., Blanco, J.-F., Raoul, Y., Mouloungui, Z., 2016. Synthesis of High-Molecular-Weight Multifunctional Glycerol Polyhydroxyurethanes PHUs. Molecules 21, 1220. https://doi.org/10.3390/molecules21091220

Peng, X., Li, Y., Zhang, G., Zhang, F., Fan, X., 2013. Functionalization of Graphene with Nitrile Groups by Cycloaddition of Tetracyanoethylene Oxide. Journal of Nanomaterials 2013, e841789. https://doi.org/10.1155/2013/841789

Rao, Y., Ogitani, S., Kohl, P., Wong, C.P., 2002. Novel polymer–ceramic nanocomposite based on high dielectric constant epoxy formula for embedded capacitor application. Journal of Applied Polymer Science 83, 1084–1090.

Schulze, K.A., Zaman, A.A., Söderholm, K.-J.M., 2003. Effect of filler fraction on strength, viscosity and porosity of experimental compomer materials. Journal of dentistry 31, 373–382.

Shin, H.S., Ra, S.H., Kim, Y.S., Kim, H.H., Choo, H.S., Lee, J.W., 2007. Method of manufacturing multilayered ceramic capacitor by spin coating and multilayered ceramic capacitor.

Strengers, Y., 2013. Peak electricity demand and social practice theories: Reframing the role of change agents in the energy sector, in: The Global Challenge of Encouraging Sustainable Living. Edward Elgar Publishing.

Sun, Z., Li, Y.H., Wang, P., Li, Z.X., Luo, Y.J., Qu, P., 2014. Parameter design principle of the capacitors and inductors in the power electronic transformer based on MMC, in: 2014 17th International Conference on Electrical Machines and Systems (ICEMS). IEEE, pp. 2445–2448.

Wang, Z., Li, H., Hu, H., Fan, Y., Fan, R., Li, B., Zhang, J., Liu, H., Fan, J., Hou, H., 2020. Direct observation of stable negative capacitance in SrTiO3@ BaTiO3 heterostructure. Advanced Electronic Materials 6, 1901005.

Wang, Z., Zhou, W., Sui, X., Dong, L., Cai, H., Zuo, J., Liu, X., Chen, Q., 2018. Dielectric studies of al nanoparticle reinforced epoxy resin composites. Polymer Composites 39, 887–894.

Zak, A.K., Razali, R., Majid, W.A., Darroudi, M., 2011. Synthesis and characterization of a narrow size distribution of zinc oxide nanoparticles. IJN 6, 1399–1403. https://doi.org/10.2147/IJN.S19693

Zhang, S.S., 2020. Dual-Carbon Lithium-Ion Capacitors: Principle, Materials, and Technologies. Batteries & Supercaps.